14th Australasian Fluid Mechanics Conference
Adelaide University, Adelaide, Australia
10-14 December 2001

The Structure of Round Zero-Net-Mass Flux Jets

J. E. Cater and J. Soria

Department of Mechanical Engineering
Monash University, Victoria, 3800 AUSTRALIA

Abstract

This paper presents the results of an experimental investigation of the structure of circular zero-net-mass flux (ZNMF) jets at a source Reynolds number of $Re_0 = 10^4$. These jets are generated by a piston oscillating in a cavity behind a circular orifice. Cross-correlation digital particle image velocimetry (CCDPIV) was used to measure instantaneous two-dimensional in-plane velocity fields in the far-field of the jets. The mean flow quantities of the ZNMF jets are compared with measurements for 'equivalent' continuous jets in the same apparatus. The results show a larger spreading rate for the ZNMF jets. The out-of-plane vorticity fields were also investigated to gain an understanding of the mechanisms responsible for the difference in spreading rate. A simple model of the velocity profile at the generator is also presented that explains the known behaviour of the velocity field in the developing region of the flow.

Introduction

The entrainment of round jets, and the associated mixing is of considerable importance to many fluid devices, such as the chambers of combustors. As noted by Wygnanski [9], the decay of the jet, and hence the radial spread is sensitive to the initial conditions, which has led others to investigate the effects of different geometries and imposed excitations to enhance or suppress the mixing of the jet. One such area of study is the investigation of pulsing jet flows, where the supply of external fluid is not steady. These jets consist of periodic flow oscillations super-imposed on a mean continuous stream. A comparison of round fully-pulsed jets was performed in the experimental work of Bremhorst [1].

A special class of pulsing jet flows are zero-net-mass-flux (ZNMF) jets (also called synthetic jets), which are generated by a mechanism that pulses the flow without net mass injection into the system. However, the fundamental difference in the fluid mechanics between a ZNMF jet and a fully pulsed jet during formation is the period when the flow direction at the generator is reversed. The study of ZNMF jets is closely related to other zero-net-mass flows, such as the flows generated by acoustic streaming.

ZNMF jets have been studied numerically in Kral [6]. This study investigated the behavior of two-dimensional laminar and turbulent ZNMF jets as compared to steady and fully-pulsed jets. The flows were classified according to the time-averaged momentum of the jets over half the period. At low source Reynolds numbers the simulated flow was identified from vorticity fields to be a series of laminar vortex pairs. The flow within the generation cavity was not simulated, and a 'top-hat' profile, with a periodic magnitude was chosen as the inflow condition to the simulation. The top-hat profile is often used in analytical studies of continuous jet behavior since analytic similarity solutions for the far-field behavior are well known. Mean velocity profiles were only qualitatively in agreement with the experimental results of Smith [8] in the near-field region. However, the agreement became more satisfactory at large distances from the orifice. Rizzetta [7] extended the domain of ZNMF jet simulations to three dimensions in an attempt to match more closely the physics of the fluid mechanism responsible for the breakup of jets in the experiments of Smith [8]. However, resource limitations prevented the simulation of rectangular jets with the same aspect ratio. This work also simulated the cavity flow for two different cavity depths, in an attempt to explain the differences between the experimental studies and the results of Kral [6]. The driving boundary was simulated by a sinusoidal inflow, but the resultant motion through the orifice was found to be non-similar in time. This was attributed to the formation of regions of vorticity within the cavity. Laminar simulations produced a series of laminar rings without the formation of a continuous stream. The single turbulent case simulated showed poor agreement with experimental velocity measurements.

The present study is concerned with the velocity evolution and mixing properties of round turbulent ZNMF jets, for which no data is presently available.

Method

The jets were formed by discharging water from the circular cylinder of inner diameter $D_p = 50\ mm$ through an orifice into the center of an end wall of the tank using a piston. An orifice plate with an inner diameter of $D_0 = 2\ mm$ was mounted at the connection between the tube exit and the tank to reduce the scale of the jet and to force the flow to separate on both the forward and suction stroke. The resulting contraction ratio between the cross-sectional area of the piston and the area of the orifice is held constant during the jet study at $A_R = 625$. Jets are matched based on the RMS velocity of the actuator. This is equivalent to the approach taken in Bremhorst [1] and Cater [2].

Particle image velocimetry is used throughout this investigation to resolve in-plane velocity fields without intrusion into the flow. To perform PIV the water in the tank was seeded with nylon spheroids of nominal diameter 28 μm with a specific gravity of 1.03. The particles were illuminated by two Spectra Physics Quanta Ray GCR170 Nd:YAG lasers that can produce an energy of 400 mJ at a wavelength of 532 nm. These lasers have a pulse width of 6 ns and the temporal pulse separation between the two lasers was variable between 187 μs - 83.4 ms. The laser beams were aligned at orthogonal states of polarization and the beam paths were combined using a polarizing beam splitter plate operating at Brewster's angle of 53.4^0.

The digital image acquisition was performed using a PCO SensiCam digital camera with a 1024×1280 pixels CCD array capable of a maximum acquisition rate of 4.5 full–frame pairs per second. The camera is operated in "Double-Short" double shuttered mode using the proprietary SensiControl software V4.03 under the Microsoft Windows NT operating system V4.00.

A multi-grid cross-correlation PIV analysis was used to capture a range of scales in the flow. This technique entails a

repeated analysis of image pairs using a grid of progressively smaller correlation regions across the imaged domain. An estimate of the velocity was used to offset each interrogation region based on the vector calculated from the previous grid. The largest interrogation region size used was a square, 64 $pixels \times 64\ pixels$, the smallest size window used measured 32 $pixels \times 32\ pixels$. At the finest grid size, the overlap of interrogation regions is 50 %.

Results

The extent of the flow was initially visualized with a fluorescent dye marker and recorded using a Pulnix analog video camera and a VHS video recorder. The dye used was Kiton Red 620, which fluoresces orange when illuminated by light with a wavelength of 532 nm. A plane of flow was illuminated with a 200 mW continuous laser spread out into a sheet for the flow visualization. Individual video frames were captured on video tape then digitized to a 256 level grey-scale image. An example of the resulting instantaneous images is shown in figure 1. To preserve zero-net-mass injection during data acquisition, the dye was initially injected to displace the fluid in the cavity behind the orifice plate. The fluid was then left to settle for several minutes before the initiation of the piston motion. The relative spread of the jets has been shown with lines that depict the mean boundary of the visible dye. The apparent spreading rates in figure 1 are 0.1 for the continuous jet and 0.13 for the ZNMF jet at $Re_0 = 10^4$.

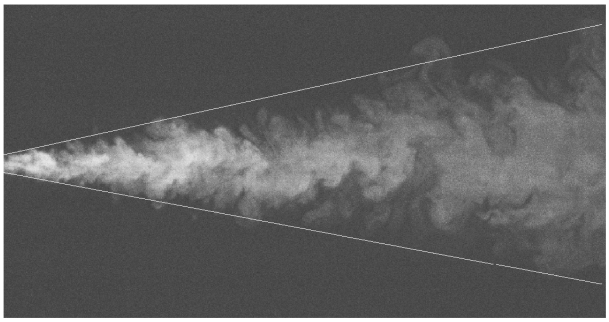

(a)

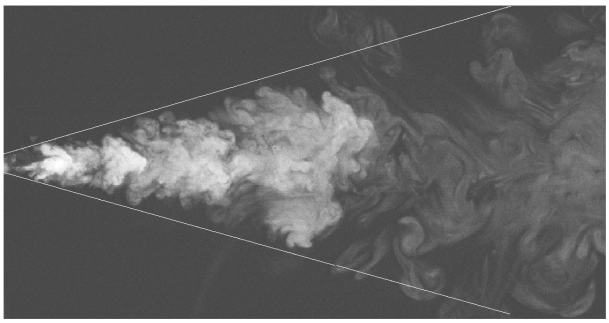

(b)

Figure 1: Digitized flow visualisation of fluorescent dye marker for (a) a continuous jet, $Re_0 = 10^4$ and (b) a ZNMF jet $Re_0 = 10^4$, $St_0 = 0.0015$. The imaged domain measures 32 $D_0 \times 16\ D_0$. The diagonal lines drawn on the images indicate the apparent mean boundary of the dye flow. The approximate spreading rates are; (a) $S_b \approx 0.1$ & (b) $S_b \approx 0.13$.

Figure 2 shows profiles of mean axial velocity for a ZNMF jet and the equivalent continuous jet at $Re_0 = 10^4$ at an axial distance of 60 D_0. The velocity is non-dimensionalised by the effective velocity at the orifice U_0, and the radial displacement is non-dimensionalised by the orifice diameter, D_0. This figure shows the difference in the mean far-field flow.

The continuous jet has a centerline velocity that is 4 times greater than the ZNMF jet at $x = 60\ D_0$. The half-width of the continuous jet is approximately $r_{\frac{1}{2}} = 5\ D_0$, whereas the ZNMF jet has a half-width closer to $r_{\frac{1}{2}} = 6\ D_0$.

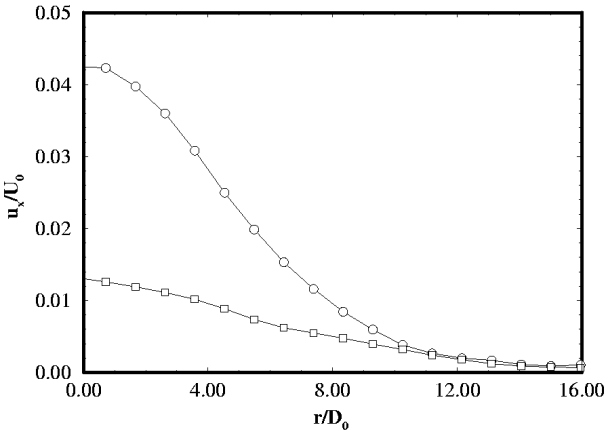

Figure 2: Non-dimensionalised (but non-normalised) profiles of axial velocity $\overline{u_x}/U_0$, at $x = 60\ D_0$ for jets at $Re_0 = 10^4$. Continuous jet [O], ZNMF jet, $St_0 = 0.0015$ [□].

Figure 3 shows the same data as figure 2, normalised by the centerline velocity and the similarity variable, $\eta = r/x$. The velocity fit to the data of Hussein [4] and the Gaussian profile given by equation 1 are also shown for comparison. It has been found that all mean stream-wise velocity profiles within the domain collapse to a Gaussian-shaped distribution [2].

$$\frac{\overline{u_x}}{U_0}(\eta) \approx \exp\left(-C\eta^2\right) \tag{1}$$

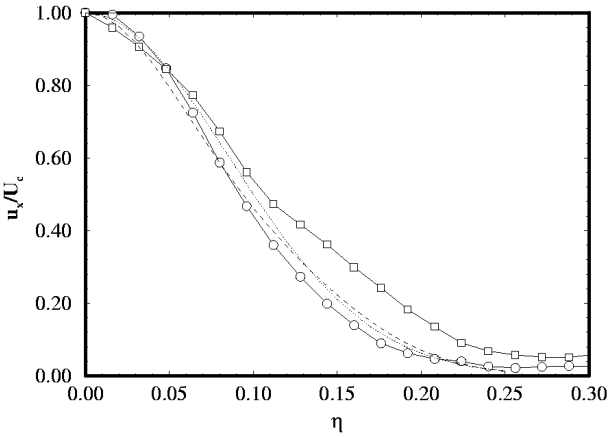

Figure 3: Normalized profiles of axial velocity $\overline{u_x}/U_c$, at $x = 60\ D_0$ for jets at $Re_0 = 10^4$. Continuous jet [O], ZNMF jet, $St_0 = 0.0015$ [□], Hussein [4] [– –] & Gaussian distribution [· · ·].

The continuous jet distribution is slightly narrower than the experimental curve fit of Hussein [4] and the Gaussian distribution. This result is consistent with a loss of axial momentum. The difference between these distributions is most noticeable between $0.1 \leq \eta \leq 0.2$.

Figure 4 shows contours of the out-of-plane vorticity $\omega_\theta = \partial u_r/\partial x - \partial u_x/\partial r$, for the two jets in an $x - r$ plane. The

figure shows that the continuous jet has higher values for vorticity at every section. There is otherwise no distinguishing feature that differentiates the two distributions.

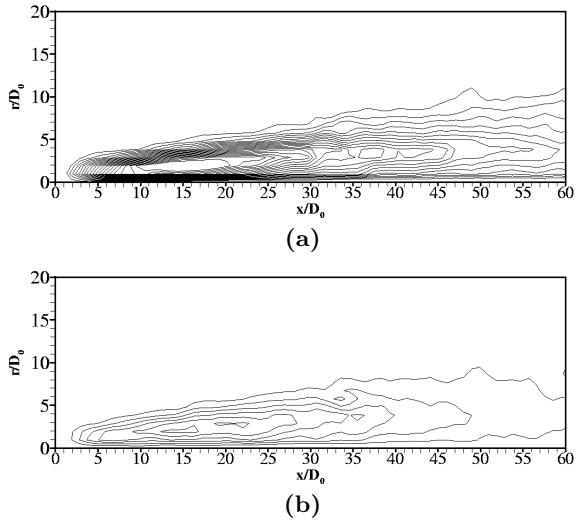

Figure 4: Mean, non-dimensional vorticity $\overline{\omega_\theta} D_0/2U_0$ at levels of 5×10^{-4}, for jets at $Re_0 = 10^4$. (a) Continuous jet, (b) ZNMF jet, $St_0 = 0.0015$.

The global mean properties of the jets are shown in table 1 compared to the analytical values for a top-hat initial velocity profile, where S_u is the decay rate of the mean centerline velocity, such that $U_0/U_c = S_u x/D_0$. The LDA measurements of Hussein [4] are also shown since this data satisfies the equations of motion to second order, and can be regarded as being representative of real unconfined axisymmetric jets.

Table 1: Jet Far-Field Properties

	Re_0	S_u	$\eta_{\frac{1}{2}}$
Analytical Model	-	0.167	0.100
Hussein et. al.[4]	10^5	0.172	0.094
Continuous Jet	10^4	0.178	0.092
ZNMF Jet	10^4	1.213	0.107

The values show that the decay of the ZNMF jet is seven times greater than the continuous jet in this facility. These measurements confirm the inference from the flow visualisation that the spreading rate of the ZNMF jets is greater.

Discussion

A previous analytical study by George [3] has shown that the scaling constants S_u and $\eta_{\frac{1}{2}}$ are facility dependent and hence the far-field remains forever dependent on the source Reynolds number and the initial jet radial velocity profile. Within an apparatus the far-field behavior is determined primarily by the initial momentum flux through the orifice and the turbulence intensity. Thus, the geometry of the cavity behind the orifice will also have some effect on the bulk flow due to its influence on the exit velocity profile at the orifice. Different velocity profiles reflect different effective formation geometries.

Therefore, to understand the differences in the structure of ZNMF jets and continuous jets it is necessary to make measurements at the generator. However, experimental limitations prevent PIV measurements at the orifice or within the cavity.

Velocity Profile Model

The mean velocity profile u_x(r) of a ZNMF jet at the orifice is unknown from these, or any previous experimental data. The only insight available for the shape of the mean profile is available in the results of the computational study by Rizzetta [7]. However, a simple model can be constructed to match the profiles given by Rizzetta and to examine the influence of different parameters.

The first limitation upon the shape of the velocity profile is imposed by the principle of conservation of mass, for a ZNMF jet the mean velocity flow through the orifice must be zero such that $2\pi \int_0^{R_0} u_x(r) r dr = 0$, where R_0 is the radius of the orifice. The second requirement is imposed from experimental observation of the flow field, that the mean centerline velocity has a positive value, specified by U_c. This gives the condition $u_x(0) = U_c$. At the orifice lip the flow must satisfy the no-slip condition given by $u_x(R_0) = 0$. Assuming axi-symmetric flow, the derivative at the centerline ($r = 0$) must be zero so that $u_x{}'(0) = 0$, where prime ('$\prime$') denotes the derivative with respect to r. An additional parameter can also be specified to take account different geometries, which is the radial velocity gradient at the orifice edge k, so that $u_x{}'(R_0) = k$.

The simple polynomial expression given by equation 2 can be used to approximate a mean velocity profile at the orifice that conforms to the these requirements, where C_i are constants.

$$\frac{u_x}{U_c} = f\left(\frac{r}{R_0}\right)$$
$$= C_0 + C_1\left(\frac{r}{R_0}\right) + C_2\left(\frac{r}{R_0}\right)^2 + C_3\left(\frac{r}{R_0}\right)^3 + C_4\left(\frac{r}{R_0}\right)^4 \quad (2)$$

The solution to this expression is a family of equations with k as the governing parameter as shown in equation 3.

$$\begin{aligned} C_0 &= 1 \\ C_1 &= 0 \\ C_2 &= -12 + 2k \\ C_3 &= 20 - 5k \\ C_4 &= -9 + 3k \end{aligned} \quad (3)$$

Examples of this family of velocity profiles are shown in figure 5 for different values of k. The value of the second derivative at the centerline is determined by the value of $2C_2 = -24 + 4k$. If $k < 6$ the second derivative at the axis is negative and the centerline value represents the maximum velocity of the profile. If $k > 6$ then the maximum velocity is located off-center.

The data of Rizzetta [7] suggest that the value of k is dependent on the Reynolds number and cavity depth of the generator. At high Reynolds numbers $k \gg 6$, and the off-center peak predicted by this model is seen in the resulting mean profiles.

Using this model it is relatively easy to determine the value of any quantity of interest at the orifice. For example, the approximate boundary of the jet flow at the orifice r_0, can be found by evaluating $f(\frac{r_0}{R_0}) = 0$, given $0 < r_0/R_0 < 1$.

The mean momentum of the jet flow at the orifice can be calculated by integrating the velocity profile from the axis to the jet boundary using equation 4.

$$M_j = 2\pi \int_0^{r_0} \left[f\left(\frac{r}{R_0}\right) \right]^2 r dr \quad (4)$$

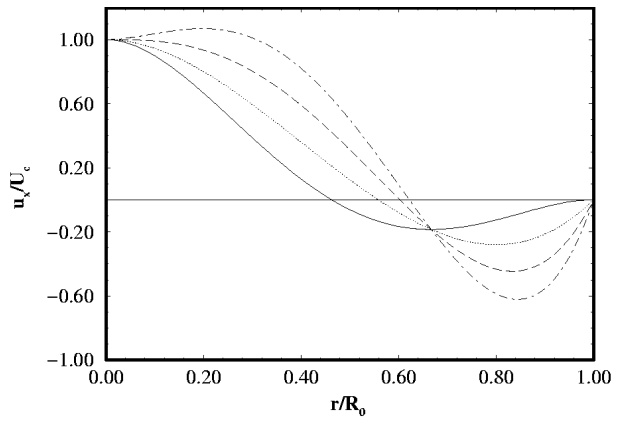

Figure 5: Orifice velocity profiles for the model of a ZNMF jet given by the polynomial expression shown in equation 2. The gradient of the profile at $r/R_0 = 1$ is specified by the constant, k. Different profiles reflect different values for k; $k = 0$ [—], $k = 3$ [· · ·], $k = 6$ [– –] & $k = 9$ [- · -].

In this case the momentum is a simple function of k, as shown in equation 5.

$$M_j = \frac{1}{35}\left(\frac{1}{24}k^2 + \frac{1}{6}k + 1\right) \tag{5}$$

By substituting a value of k which best fits the data of Rizzetta into equation 5, the momentum is found to be 16 % of that for a continuous jet with the same centerline velocity.

A ZNMF jet generated by a round piezoelectric device was investigated in James [5]. In this study a jet was produced by a piezoelectric diaphragm mounted flush with a wall and submerged in water. However, a ZNMF jet was only generated for high amplitudes of oscillation when cavitation bubbles formed at the diaphragm surface. The formation of the jet was therefore attributed to the motions caused by the periodic formation and collapse of the bubbles.

The model presented above can be used to explain this behaviour. The boundary conditions are such that a jet flow cannot be produced without a mean annulus of reverse flow at the generator. Since a flush mounted actuator does not permit a mean reverse flow at any point this may explain why the experimental study of James [5] failed to generate a ZNMF jet without cavitation. This data highlights the importance of the cavity in generating the turbulent ZNMF jet flow.

Concluding Remarks

This paper provides experimental measurements of the parameters that govern the velocity and vorticity evolution for a round turbulent ZNMF jet at the highest Reynolds number to date. It is shown that the spreading rate of the ZNMF jet is greater than a turbulent continuous jet in the same apparatus. A simple model is constructed for the mean velocity profile at the generator. This model demonstrates that the momentum of a ZNMF jet is an order of magnitude less than a continuous jet in the same environment with an equivalent actuator velocity.

Acknowledgments

The financial support of the ARC to undertake this research is greatly appreciated.

References

[1] Bremhorst, K. and Hollis, P.G., Velocity field of an axisymmetric pulsed, sub-sonic air jet, *AIAA Journal*, **28**, 1990, 2043–2049.

[2] Cater, J. and Soria J., Comparisons between Axi-Symmetric Zero-Net-Mass Flux Jets and Continuous Jets, *7th Heat and Mass Transfer Conference Australasia*, 2000, 75–80.

[3] George, W.K., The self-preservation of turbulent flows and its relation to initial and coherent structures, *Advances in Turbulence*, **Hemisphere**, 1989, 37–72.

[4] Hussein, H.J., Capp, S.P. and George, W.K., Velocity measurements in a high-Reynolds number, momentum conserving, axisymmetric, turbulent jet, *J. Fluid Mech.*, **258**, 1994, 31–75.

[5] James, R.D., Jacobs, J.W. and Glezer A., A round turbulent jet produced by an oscillating diaphragm, *Phys. Fluids*, **8**, 1996, 2484–2495.

[6] Kral, L.D., Donovan, J.F., Cain, A.B. and Cary, A.W., Numerical simulation of synthetic jet actuators, *4th AIAA Shear Flow Control Conference*, **AIAA**, 1997.

[7] Rizzetta, D.P., Visbal, M.R. and Stanek, M.J., Numerical Investigation of Synthetic Jet Flow-fields, *AIAA Journal*, **37**, 1999.

[8] Smith, B.L. and Glezer, A., Vectoring and small-scale motions effected in free shear flows using synthetic jet actuators, *AIAA Journal*, **97-0213**, 1997.

[9] Wygnanski, I. and Fieldler, H., Some measurements in the self-preserving jet, *Phys. Fluids*, **38**, 1969, 577–612.